AFRL-RW-EG-TP-2010-073

# Modeling and Characterization of PMMA for High Strain-Rate and Finite Deformations (Postprint)

**Eric B. Herbold**
**Jennifer L. Jordan**
**M.E. Nixon**

**Air Force Research Laboratory**
**Munitions Directorate**
**Eglin AFB FL 32542-5910**

**Naresh N. Thadhani**

**School of Material Science & Engineering**
**Georgia Institute of Technology**
**Atlanta GA 30332-0254**


**May 2010**

 [doi 10.1063/1.3295028] This paper was presented at the Conference of the American Physical Society Topical Group on Shock Compression of Condensed Matter and published in the conference proceedings December 28, 2009, Vol 1195, pp.1237 – 1230. 

**AIR FORCE RESEARCH LABORATORY, MUNITIONS DIRECTORATE**

**Air Force Materiel Command ■ United States Air Force ■ Eglin Air Force Base**

# REPORT DOCUMENTATION PAGE

*Form Approved*
*OMB No. 0704-0188*



| **1. REPORT DATE** *(DD-MM-YYYY)* | **2. REPORT TYPE** | **3. DATES COVERED** *(From - To)* |
|---|---|---|
| 05- 2010 | Interim – Conference Paper | 18 December 2007 – 30 July 2009 |

**4. TITLE AND SUBTITLE**

Modeling and Characterization of PMMA for High Strain-Rate and Finite Deformations (Postprint)

**5a. CONTRACT NUMBER**

**5b. GRANT NUMBER**

**5c. PROGRAM ELEMENT NUMBER**
62102F

**6. AUTHOR(S)**

Eric B. Herbold, Jennifer L. Jordan, M.E. Nixon, Naresh N. Thadhani

**5d. PROJECT NUMBER**
4347

**5e. TASK NUMBER**
95

**5f. WORK UNIT NUMBER**
05

**7. PERFORMING ORGANIZATION NAME(S) AND ADDRESS(ES)**

Air Force Research Laboratory, Munitions Directorate
Ordnance Division
Energetic Materials Branch (AFRL/RWME)
Eglin AFB FL 32542-5910
Technical Advisor: Dr. Jennifer L. Jordan

**8. PERFORMING ORGANIZATION REPORT NUMBER**

AFRL-RW-EG-TP-2010-073

**9. SPONSORING / MONITORING AGENCY NAME(S) AND ADDRESS(ES)**

SAME AS BLOCK 7

**10. SPONSOR/MONITOR'S ACRONYM(S)**
AFRL-RW-EG

**11. SPONSOR/MONITOR'S REPORT NUMBER(S)**
SAME AS BLOCK 8

**12. DISTRIBUTION / AVAILABILITY STATEMENT**

Distribution A: Approved for public release; distribution unlimited. Approval Confirmation 96 ABW/PA # 96ABW-2009-0330, Dated July 30, 2009

**13. SUPPLEMENTARY**

SEE 'COVER PAGE' FOR PERTINENT METADATA INFORMATION.

**14. ABSTRACT**

The complex response of glassy polymers to high strain-rate dynamic loading necessitates accurate modeling of these events for comparison with experiments. The strain-rate, temperature and the strain softening behavior are significant and must be considered for large deformations. Several constitutive relationships are discussed in terms of their applicability to modeling PMMA in gap-tests.

**15. SUBJECT TERMS**
PMMA, constitutive model, gap-test, comp-b, dynamic deformation

| **16. SECURITY CLASSIFICATION OF:** | | | **17. LIMITATION OF ABSTRACT** | **18. NUMBER OF PAGES** | **19a. NAME OF RESPONSIBLE PERSON** |
|---|---|---|---|---|---|
| **a. REPORT** | **b. ABSTRACT** | **c. THIS PAGE** | | | Jennifer L. Jordan |
| UNCLASSIFIED | UNCLASSIFIED | UNCLASSIFIED | UL | 6 | **19b. TELEPHONE NUMBER** *(include area code)* 850-882-8992 |

**Standard Form 298 (Rev. 8-98)**
**Prescribed by ANSI Std. Z39.18**

CP1195, *Shock Compression of Condensed Matter - 2009*,
edited by M. L. Elert, W. T. Buttler, M. D. Furnish, W. W. Anderson, and W. G. Proud


# MODELING AND CHARACTERIZATION OF PMMA FOR HIGH STRAIN-RATE AND FINITE DEFORMATIONS

**E.B. Herbold[1,2], J.L. Jordan[2], M.E. Nixon[3] and N.N. Thadhani[1]**

[1]*School of Materials Science and Engineering, Georgia Institute of Technology, Love Manufacturing Building, 771 Ferst Drive, Atlanta, Georgia 30332, USA*
[2]*Energetic Materials Branch, Munitions Directorate, Air Force Research Laboratory, Eglin AFB, FL 32542, USA*
[3]*Computational Mechanics Branch, Munitions Directorate, Air Force Research Laboratory, Eglin AFB, FL 32542, USA*

**Abstract.** The complex response of glassy polymers to high strain-rate dynamic loading necessitates accurate modeling of these events for comparison with experiments. The strain-rate, temperature and the strain softening behavior are significant and must be considered for large deformations. Several constitutive relationships are discussed in terms of their applicability to modeling PMMA in gap-tests.

**Keywords:** PMMA, constitutive model, gap-test, comp-b, dynamic deformation
**PACS:** 61.41.+e, 62.20.F-, 62.40.+i, 61.43.Bn

## INTRODUCTION

Polymethyl methacrylate (PMMA) is often used as a window material or as a barrier between a donor and acceptor explosive in shock sensitivity experiments (e.g. 'gap-tests') [1-6]. However, the response of PMMA (and glassy polymers in general) to dynamic loading is highly nonlinear due to the competition of softening (temperature and strain) and hardening (strain-rate and entropic) effects, which have been investigated in [1-10]. Strength models incorporating these effects evolved from low strain-rate processes (e.g. extrusion) in [7] with strain rates in the range of $10^{-4}$–1 $s^{-1}$. More recent advances of this model focus on high strain-rate processes (e.g. the Taylor impact test) with rates as high as $10^{5}$ $s^{-1}$ [8, 9].

However, for strain rates at or above $10^{6}$ $s^{-1}$ the compressibility of the polymer becomes significant and the constitutive models must incorporate an appropriate equation of state. One such constitutive model has been developed [4] for modeling the behavior of PMMA in the high pressure and strain-rate regime. It accounts for the nonlinear nature of the shear strains and the relaxation present in shock wave profiles but does not incorporate thermal effects. A more recent constitutive model captures the equation of state and the prominent thermal effects derived from the polymer chain structure [8].

This work discusses the first steps toward modifying the Mulliken-Boyce strength model [7] for shock wave experiments. We also present gap tests using comp-B as the donor explosive and PMMA as the 'attenuator' with numerical calculations for comparison.

The Mulliken-Boyce constitutive model is appropriate for glassy polymers under high strain rate loading conditions. It has been implemented in a Lagrangian finite element code (EPIC, 2006 version [11]) to capture the rate and temperature effects in polymers under high strain rates [8,9]. As discussed in [5,6] the strength of PMMA is important to include in gap test simulations in order to accurately predict the pressure at the interface of the PMMA and receptor explosive.

The implementation of the Mulliken-Boyce model is depicted in Fig. 1, which shows two distinct branches denoted A and B. In branch A, there are two sub-branches that correspond to the glass ($\alpha$) and viscoelastic ($\beta$) transitions apparent in the storage and loss moduli in dynamic mechanical analysis (DMA) [8]. A modification to this model

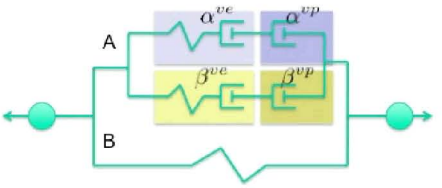


**Figure 1.** Rheological schematic of the modified Mulliken-Boyce model [8].

is the addition of a viscoelastic dashpot to each sub-branch of 'A'. The model was originally constructed to use DMA data for the elastic moduli, but mesh dependent instabilities occur in the calculations due to adjacent elements having different moduli and sound speeds [9]. The viscoplastic dashpots (denoted '*vp*') are somewhat of a misnomer since a yield criterion for the material is not explicitly defined, but the notation is maintained for consistency with the original model.

The kinematics of this model require that the total deformation in each branch is equal

$$\mathbf{F} = \mathbf{F}_{A\alpha} = \mathbf{F}_{A\beta} = \mathbf{F}_{B} \tag{1}$$

where $\mathbf{F}$ is the deformation tensor and the subscripts denote the branch shown in Fig. 1. The deformation tensor may be multiplicatively decomposed into elastic and thermoplastic parts, $\mathbf{F} = \mathbf{F}^{e}\mathbf{F}^{thp}$, where $\mathbf{F}^{thp} = \mathbf{F}^{th}\mathbf{F}^{p}$ and it is assumed that the plastic deformation is an isochoric process (i.e. $\det|\mathbf{F}^{p}| = \mathbf{1}$ [4,7-9]). The velocity gradient in branch A is

$$\mathbf{L}_{A*}=\mathbf{L}^{e}_{A*}+\mathbf{F}^{e}_{A*}\mathbf{L}^{thp}_{A*}\left(\mathbf{F}^{e}_{A*}\right)^{-1} \tag{2}$$

where $(*)$ denotes either $\alpha$ or $\beta$. In Eq. (2) the thermoplastic velocity gradient is defined

$$\mathbf{L}^{thp}_{A*}=\mathbf{D}^{thp}_{A*}+\mathbf{W}^{thp}_{A*}+\alpha\dot{\theta}\mathbf{I} \tag{3}$$

where $\mathbf{D}^{thp}$ is the thermoplastic rate of deformation tensor, $\alpha$ is the coefficient of thermal expansion, $\theta$ is the temperature and $\mathbf{I}$ is the identity tensor. It is assumed that the plastic spin tensor $\mathbf{W}^{thp} = \mathbf{0}$. In Eq. (3) the thermoplastic rate of deformation tensor is coaxial with the branch deviatoric stress,

$$\mathbf{D}^{thp}_{A*}=\dot{\gamma}^{p}_{A*}\mathbf{N}^{p}_{A*}+\alpha\dot{\theta}_{A*}\mathbf{I} \tag{4}$$

where $\mathbf{N}^{p}_{A*}=\boldsymbol{\sigma}'_{A*}/|\boldsymbol{\sigma}'_{A*}|$ is the normalized deviatoric stress tensor and $\dot{\gamma}^{p}_{A*}$ is the plastic shear strain rate,

$$\dot{\gamma}^{p}_{A*}=2\dot{\gamma}^{p}_{0,A*}\exp\left(\frac{\Delta G_{A*}}{k\theta}\right)\sinh\left[\frac{\Delta G_{A*}}{k\theta}\frac{\tau_{A*}}{s_{A*}+\alpha_{p,A*}p}\right]. \tag{5}$$

In Eq. (5), $\dot{\gamma}^{p}_{0,A*}$ is the initial plastic strain rate parameter, $\Delta G_{A*}$ is the activation energy [12], $k$ is Boltzmann's constant, $\theta$ is the current temperature, $s_{A*}$ is the temperature and rate dependent yield strength and $\tau_{A*}=\sqrt{(\boldsymbol{\sigma}'_{A*}:\boldsymbol{\sigma}'_{A*})/2}$ is a measure of equivalent stress. Pressure dependent yield is also included in Eq. (5) with the parameter $\alpha_{p,A*}>0$.

The temperature and rate dependent strength evolves according to the relation,

$$\dot{s}_{A*}=h\left(1-s_{A*}/s_{ss,A*}\right)\dot{\gamma}^{p}_{A*} \tag{6}$$

where $h$ is a strain softening parameter and $s_{ss,A*}$ denotes the 'preferred' strength [9]. In Eq. (4) the rate of temperature change is

$$\dot{\theta}=\frac{1}{\rho C_{p}}\left\{\mathrm{tr}\left[\bar{\boldsymbol{\sigma}}_{A\alpha}\left(\mathbf{D}^{p}_{A\alpha}+\bar{\mathbf{D}}^{ve}_{A\alpha}\right)\right]+\mathrm{tr}\left[\bar{\boldsymbol{\sigma}}_{A\beta}\left(\mathbf{D}^{p}_{A\beta}+\bar{\mathbf{D}}^{ve}_{A\beta}\right)\right]\right\} \tag{7}$$

where $\boldsymbol{\sigma}$ is the Cauchy stress tensor, $\mathbf{D}^{p}$ is the first term in Eq. (4), $\rho$ and $C_p$ are the density and specific heat. The overbars in Eq. (7) indicate that the tensor resides in the elastically unloaded configuration. The viscoelastic energy loss is accounted for in Eq. (7) with,

$$\mathbf{D}^{ve}_{A*}=\tau_{A*}\mathbf{N}^{p}_{A*}/\eta_{A*}=\left(\tau_{A*}E_{A*}\bar{t}_{A*}\right)\mathbf{N}^{p}_{A*} \tag{8}$$

where $\eta_{A*}$ is a viscosity parameter, $E_{A*}$ is Young's modulus and $\bar{t}_{A*}$ is the relaxation time. The viscoelastic parameters for the subbranches are constants found from DMA data by a process described in [9]. The elastic constants are taken as the 'cold' values of the DMA data, however the model must incorporate compressibility effects above the Hugoniot elastic limit (0.75 GPa [2]) for comparison with experiments.

In the integration scheme for this constitutive model, the Jaumann rate was used to update the stresses. This stress rate may be expressed as a function of the rate of deformation tensor,

$$\dot{\boldsymbol{\sigma}}_{A*}=\mathbf{C}^{\sigma J}_{el,A*}\left(\mathbf{D}-\mathbf{D}^{ev}_{A*}-\mathbf{D}^{thp}_{A*}\right) \tag{9}$$

using an isotropic tangent stiffness modulus $\mathbf{C}^{\sigma J}_{el,A*}$.

Branch 'B' in Fig. 1 is the polymer chain network back-stress describing entropic resistance to molecular alignment. The Arruda-Boyce 8-chain model was used for the back-stress [13],

$$\boldsymbol{\sigma}_{B}=\frac{\sqrt{N}C_{R}}{3\lambda^{p}_{chain}}L^{-1}\left(\frac{\lambda^{p}_{chain}}{\sqrt{N}}\right)\bar{B}', \tag{10}$$

where $\sqrt{N}$ is the limiting (or locking) value of stretch, $\lambda^{p}_{chain}=\sqrt{\mathrm{tr}(\bar{B})/3}$ is a measure of plastic stretch, $C_R$ is the rubbery modulus $L^{-1}(\bullet)$ is the inverse Langevin function, and $\bar{B}'=|F|^{-2/3}FF^{T}$ is the deviatoric

**Table 1.** List of parameters for the modified Mulliken-Boyce model for PMMA.

| | Value | Units | | Value | Units |
|---|---|---|---|---|---|
| $E_{A\alpha}$ | 3386 | MPa | $s_{ss\alpha}/\ s_{0\alpha}$ | 0.73 | – |
| $E_{A\beta}$ | 1748 | MPa | $\alpha_{th}$ | $7.4\times10^{-5}$ | 1/K |
| $\nu$ | 0.35 | – | $\alpha_{p,A*}$ | 0.26 | – |
| $\theta_0$ | 298 | K | $\dot{\gamma}^p_{\alpha,0}$ | $3.2\times10^{13}$ | 1/s |
| $\overline{t}_{A\alpha}$ | 1979 | s | $\dot{\gamma}^p_{\beta,0}$ | $3.6\times10^{4}$ | 1/s |
| $\overline{t}_{A\beta}$ | 1573 | s | $\Delta G_\alpha$ | $3.6\times10^{-19}$ | J |
| $C_R$ | 14 | MPa | $\Delta G_\beta$ | $6.4\times10^{-20}$ | J |
| $h_\alpha$ | 300 | MPa | $N$ | 4.84 | – |
| $h_\beta$ | 0 | MPa | | | |

portion of the left-isochoric Cauchy-Green deformation. Finally, the total stress is composed from each branch $\sigma = \sigma_{A\alpha} + \sigma_{A\beta} + \sigma_B$.

The values for the parameters were found using a genetic algorithm in MatLab® and are listed in Table 1 [14]. The parameters are fit using experimental data at different temperatures and (constant) strain rates. It is assumed that with these parameters the model is sufficient to describe more complex simulations such as the Taylor bar impact experiment shown in Fig. 2.

Gap tests have been performed for model validation. At this stage it is useful to investigate how well calculations compare to the experimental data using a cubic Mie-Gruneisen equation of state and an elastic-perfectly plastic strength model. This is an important step for validation of the experimental data using parameters from well documented sources [11] and serves as a benchmark test for the modified constitutive model.

In each experiment a 3" diameter PMMA cylinder is placed below a 1" thick pad of Comp-B explosive. A streak camera was used to record the location of the shock front in time and space by rotating an image of a flattened portion, or window, of the PMMA onto a film strip. The setup was backlit by a PBXN-110 pad (or Argon candle). The streak images were processed using an algorithm written in IGOR to extract the location and time (or x-t plots) of the shock front for comparison with numerical calculations.

Six PMMA samples were created for these experiments. Each had a flat portion machined

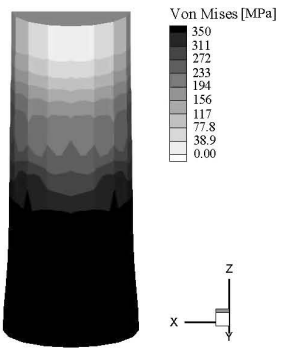


**Figure 2.** Von Mises stress distribution in a simulated Taylor impact test at 250 m/s. The image is captured at the point of maximum compression.

along the side to allow light through a slit into the camera. One of the samples (09045) was 'polished' by flame while the other five were mechanically polished. Also, a crack was observed on the bottom of one of the samples (09041). Cracks may act a source of enhanced energy dissipation (hot-spots) within the material due to crack-tip instabilities in PMMA [15-17].

In Fig. 3 the streak records are shown. The time increases on the horizontal axis from left to right and the shock front, which is the uppermost bright portion of the curved section, passes through the cylinder from the bottom to the top of the image.

Simulated pressure-time profiles at various points in the Comp-B and PMMA are computed in a simulation of the experimental setup using EPIC06 [11]. The cubic form of the Mie-Gruneisen equation of state is used for this calculation

$$P = \left(k_1\mu + k_2\mu^2 + k_3\mu^3\right)\left(1 - \Gamma\mu/2\right) + \Gamma E_s\left(1+\mu\right) \quad (11)$$

where $\mu = \rho/\rho_0 - 1$, $E_s$ is the internal energy per unit volume, $k_1 = 5.85\times10^{10}$, $k_2 = 3.541\times10^{11}$, $k_3 = 1.74\times10^{10}$, and $\Gamma = 0.8$ is the Gruneisen coefficient. The yield strength was $\sigma_y = 6.48$ MPa.

Figure 4 shows the experimental results taken from the streak images compared to the numerical calculation. The numerical part of the figure is a contour plot of the pressure with the origin located at the interface of the comp-B pad and PMMA.

It is clear that curves (3)-(6) (labeled from left to right) are tightly grouped together indicating a repeatable test with this batch of PMMA. Curve (2) corresponds to the 'flame-polished' sample, which


**Figure 3.** The streak image shows the propagation of a shock into PMMA. Time increases from the left to right and the propagation from bottom to top. The shock front is tracked for experimental and numerical comparison.

clearly exhibits a lower shock speed. Curve (6) is the sample with a crack at the bottom, which did not influence the shock propagation, which is probably due to its location. Curve (1) has the lowest speed of the group. It is unclear why this particular sample exhibited such a low shock speed since the cylinder was mechanically polished and free of imperfections. Overall, curves (3)-(6) match the numerical calculation well until the release wave from the edge of the cylinder reach its axis. Strength effects play an important role in predicting the time of arrival of the release wave to the center axis of the PMMA and the subsequent pressure change occurring as the shock front arrives at the interface of the acceptor explosive in gap tests [6].

In summary, a modified version of the 3-D Mulliken-Boyce model was implemented into EPIC. This model is applicable to glassy polymers in general and may be used in the future for simulations with polymers used as binders in explosive applications. The model lacks compressibility effects, which are essential in modeling high-pressure phenomena. The cubic Mie-Gruneisen equation of state predicted the shock speed well but more sophisticated strength models are necessary to better estimate the pressure wave at the interface of the acceptor explosive.

## ACKNOWLEDGEMENTS

EBH would like to thank the Florida Institute for Research in Energetics (FIRE) for support. We would like to thank Mark Grimmonpre for obtaining the shock front data from the streak images, AFRL/RWMEP and the Dynamics laboratory for the PMMA samples and experimental preparation.

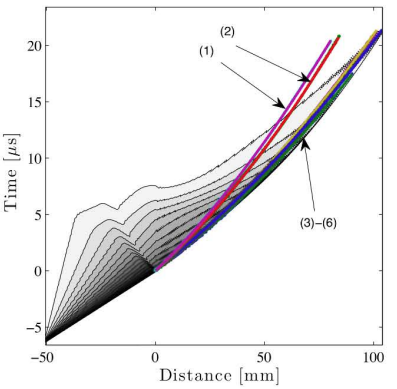


**Figure 4.** Shock front profiles for six different gap tests. The data presented in curves (1)-(6) is taken from an algorithm implemented in IGOR.

## REFERENCES

1. Barker, L.M., Hollenbach, R.E., J. Appl. Phys. **41**, 4208 (1970).
2. Schuler, K.W., Nunziato, J.W., J. Appl. Phys. **47**, 2995 (1976).
3. Millet, J.C.F., Bourne, N.K., J. Appl. Phys. **88**, 7037 (2000).
4. Menikoff, R., J. Appl. Phys. **96**, 7696 (2004).
5. Hudson, L.C. III, and Bernecker, R.R., Propellants, Explosives, Pyrotechnics **20**, 330 (1995).
6. Sutherland, G., these proceedings (2009).
7. Boyce, M.C., Parks, D.M., Argon, A.S., Mech. of Mat. **7**, 15 (1988).
8. Mulliken, A.D., and Boyce, M.C., Int. J. Solids and Structures **43**, 1331 (2006).
9. Mulliken, A.D., *Mechanics of amorphous polymers and polymer nanocomposites during high rate deformation*, Ph.D. dissertation, MIT (2006).
10. Porter, D., Gould, P.J., Int. J. Solids and Struct. **46**, 1981 (2009).
11. EPIC (2006 version) manual.
12. Ree, T., Eyring, H., J. Appl. Phys. **26**, 793 (1955).
13. Arruda, E.M., Boyce, M.C., J. Mech. Phys. Solids **41**, 389 (1993).
14. Jordan, J.L., Foley, J.R., and Siviour, C.R., Mech. Time-Depend. Mater. **12**, 249 (2008).
15. Fineberg, J., Gross, S.P, Marder, M., Swinney, H.L., Phys. Rev. B, **45**, 5146 (1992).
16. Sharon, E., Gross, S.P., Fineberg, J., Phys. Rev. Lett., **76**, 2117 (1996).
17. Washabaugh, P.D., and Hill, L.G., Shock Comp. of Cond. Matt., Proc.-2007, 727 (2007).